REPORT DOCUMENTATION PAGE

Form Approved
OMB No. 0704-0188

1. REPORT DATE *(DD-MM-YYYY)*	2. REPORT TYPE	3. DATES COVERED *(From - To)*
11/16/2014	Conference Paper - Conference Paper	1/1/0001 - 1/1/0001

4. TITLE AND SUBTITLE
Multi Scale Modeling of Continuous Aramid Fiber Reinforced Polymer Matrix Composites Used in Ballistic Protection Applications

5a. CONTRACT NUMBER

5b. GRANT NUMBER

5c. PROGRAM ELEMENT NUMBER

6. AUTHOR(S)

5d. PROJECT NUMBER

5e. TASK NUMBER

5f. WORK UNIT NUMBER

7. PERFORMING ORGANIZATION NAME(S) AND ADDRESS(ES)
Clemson University Clemson SC 242

8. PERFORMING ORGANIZATION REPORT NUMBER

9. SPONSORING/MONITORING AGENCY NAME(S) AND ADDRESS(ES)
Army Research Laboratory Aberdeen Proving Ground 20 242

10. SPONSOR/MONITOR'S ACRONYM(S)

11. SPONSOR/MONITOR'S REPORT NUMBER(S)

12. DISTRIBUTION/AVAILABILITY STATEMENT
1 1/1/0001 12:00:00 AM

13. SUPPLEMENTARY NOTES

14. ABSTRACT
This work addresses the problem of multi length scale modeling of polymer matrix composites reinforced with high specific strength, high specific stiffness continuous aramid fibers. These composite materials are commonly used in various light weight protective systems the main requirement of which is a high level of penetration resistance against high kinetic energy projectiles (e.g. bullets, exploded mine propelled soil ejecta, fragments of improvised explosive devices, turbine blades, etc.). Within the proposed multi length scale modeling approach, the following distinct length scales have been identified and their respective mechanical constitutive relations derived and parameterized: (a) molecular chain; (b) fibril;

15. SUBJECT TERMS

16. SECURITY CLASSIFICATION OF:			17. LIMITATION OF ABSTRACT	18. NUMBER OF PAGES	19a. NAME OF RESPONSIBLE PERSON
a. REPORT	b. ABSTRACT	c. THIS PAGE			19b. TELEPHONE NUMBER *(Include area code)*
U	U				

MULTI SCALE MODELING OF CONTINUOUS ARAMID FIBER REINFORCED POLYMER MATRIX COMPOSITES USED IN BALLISTIC PROTECTION APPLICATIONS

M. Grujicic [a], J. S. Snipes [a], S. Ramaswami [a], R. Yavari [a], C.-F. Yen [b], B. A. Cheeseman [b]
[a]Clemson University
241 Flour Daniel Building
Clemson SC 29634-0921

[b]Army Research Laboratory – Weapons & Materials Research Directorate
Survivability Materials Branch
Aberdeen, Proving Ground MD 21005-5069

ABSTRACT

This work addresses the problem of multi length scale modeling of polymer matrix composites reinforced with high specific strength, high specific stiffness continuous aramid fibers. These composite materials are commonly used in various light weight protective systems the main requirement of which is a high level of penetration resistance against high kinetic energy projectiles (e.g. bullets, exploded mine propelled soil ejecta, fragments of improvised explosive devices, turbine blades, etc.). Within the proposed multi length scale modeling approach, the following distinct length scales have been identified and their respective mechanical constitutive relations derived and parameterized: (a) molecular chain; (b) fibril; (c) fiber; (d) yarn; (e) fabric/ply; (f) single lamina; (g) stacked lamina; and (h) laminate. In addition, issues related to identification of the type and the extent of data generated at a finer length scale to the adjacent coarser length scale, as well as seamless integration of different length scales into a unified material model, are addressed. Finally, results are presented pertaining to the implementation of the multi scale material model into a transient, nonlinear dynamics/finite element analysis of a few simplified ballistic impact scenarios.

1. INTRODUCTION

One way polymer matrix composites are classified is as structural grade and armor grade (the subject of the present work). For the structural grade composites (SGCs), the main figures of merit are their density normalized stiffness and strength (i.e. specific stiffness and specific strength, respectively). As far as the armor grade composites (AGCs) are concerned, they are generally optimized with respect to their ballistic impact/penetration resistance, i.e. with respect to their energy absorbing capability. Their most commonly cited figure of merit is their "ballistic limit," which is defined as the critical velocity below which no full perforation takes place [e.g. 1]. To maximize this figure of merit, AGCs are generally "resin starved," i.e. they are not fully impregnated with resin. Consequently, the reinforcing fibers are not highly constrained by the surrounding polymeric matrix and, hence, do not suffer extensive cutting/shearing during the transverse impact of a projectile onto an AGC panel.

Development of the AGCs is traditionally carried out using legacy knowledge and extensive

fabricate and test procedures. Since this approach is not only economically unattractive, but is often associated with significantly longer lead times, it has gradually become complemented by the appropriate cost and time efficient Computer Aided Engineering (CAE) analyses. However, the tools used suffer from a number of deficiencies/limitations which prevent these analyses from being more widely utilized. In the context of the use of CAE analyses for development of the AGCs, it is well established that one of the main deficiencies stems from the inability of the most currently available material models to realistically represent the response of these materials under high deformation rate, large strain, high pressure loading conditions, the conditions typically encountered during projectile impact events. One of the reasons for the indicated shortcomings of the present material models is a lack of inclusion of the contribution of various phenomena and processes occurring at different length/time scales to the overall behavior/performance of the material.

AGCs are quite complex materials, and this complexity can be linked to the following main sources: (a) they contain a hierarchical/multi length scale microstructure/architecture; (b) their mechanical response is often quite nonlinear and rate /time /temperature /pressure dependent; and (c) they are associated with a multiplicity of complex phenomena/processes (e.g. filament twisting/buckling, inter filament friction and sliding, etc.). A detailed examination of the intrinsic makeup of this class of materials typically reveals the existence of eight well defined microstructural length scales [e.g. 2]. Schematics of these length scales (along with labels denoting the main microstructural constituents/features), starting from the finest (i.e. molecular chain level) length scale, are provided in Figure 1. A more detailed description of the material microstructure/architecture and the corresponding material models at each of the length scales listed in Figure 1 can be found in [2–6].

Careful examination of Figure 1 suggests that the eight length scales could be grouped in the following way: (a) *Molecular and Fibril length scales* – At these length scales, the material is represented as an ensemble of interacting constituent particles (atoms/ions); (b) *Fiber, Yarn, Single ply length scales* – At these length scales, the materials are treated as being of a continuum character, while the structural constituents (e.g. fibers/yarns, fabric unit cells) are treated as being discrete; and (c) *Single lamina, Stacked lamina and Laminate length scales* – At these length scales, both the material and the structural elements (e.g. laminae, lamina/lamina interfaces, etc.) are treated as being of a continuum character. This grouping is adopted in the present work.

2. MOLECULE AND FIBRIL SCALE MODELING

Material models falling into this class will be discussed within the context of *p*-phenylene terephthalamide (PPTA) polymeric filaments such as Kevlar®, Twaron®, etc.

Molecular level: A pictorial representation, with labels, of a single PPTA repeat unit (in its common trans-configuration, which promotes formation of lower energy stretched out/extended molecules/chains), consisting of two phenylene rings/moieties joined by two amide linkages, is shown in Figure 2.

Fibril scale: The presence of large numbers of nearly parallel (fairly rigid) molecules with a nearly linear back bone structure promotes, in turn, formation of (crystalline or paracrystalline) PPTA fibrils. Amide linkages of adjacent PPTA chains tend to form hydrogen bonds.

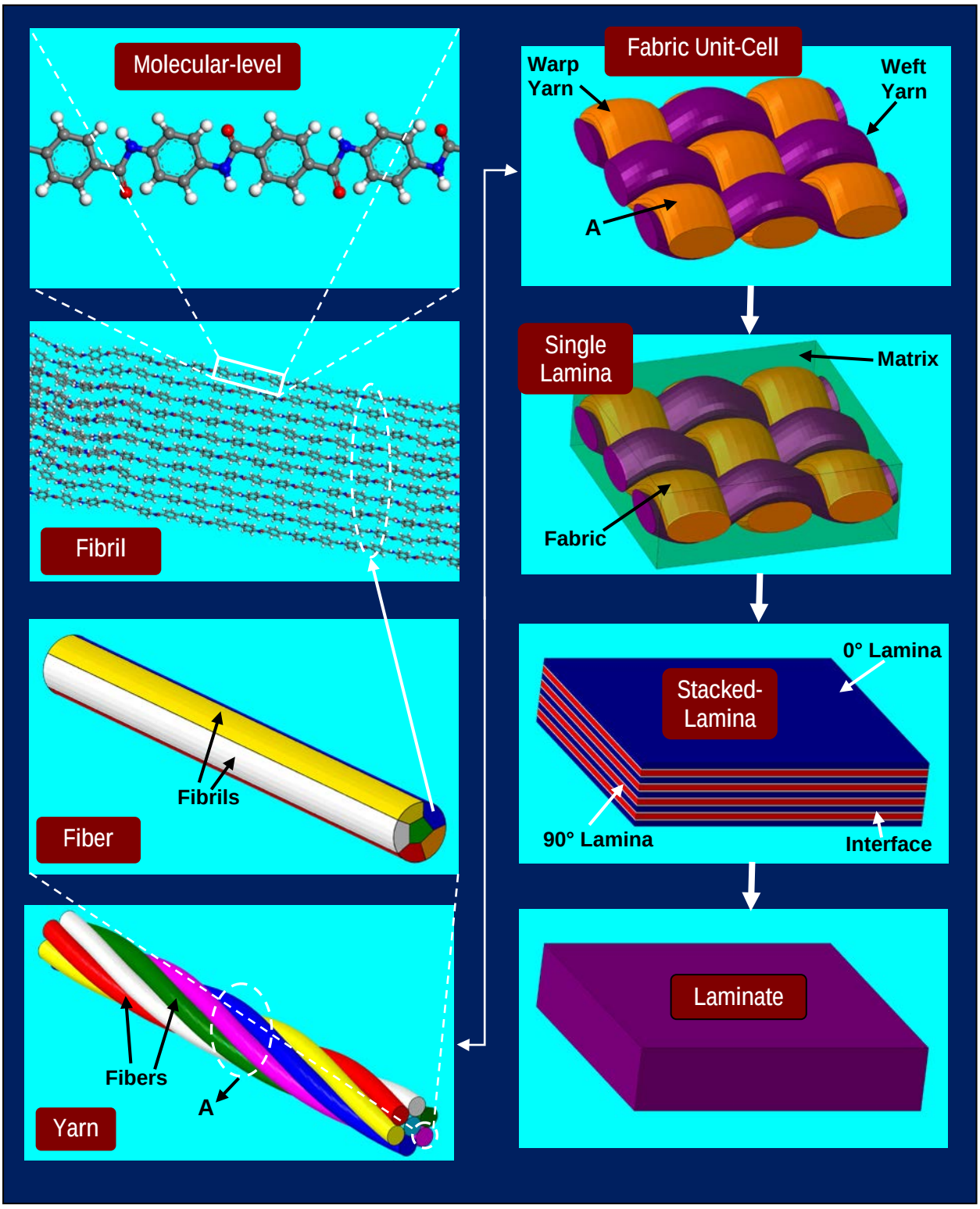

Figure 1. Eight length scales encountered in the study of polymer matrix composite materials reinforced with high performance fiber based structures.

Such bonds are formed laterally between parallel PPTA chains, creating "*sheet like*" structures within the fibrils. PPTA fibrils are commonly found to have a crystalline structure consisting of stacked sheets. However, while hydrogen bonding plays a key role in the formation of the sheets, its contribution to the inter sheet bonding is generally considered to be minor.

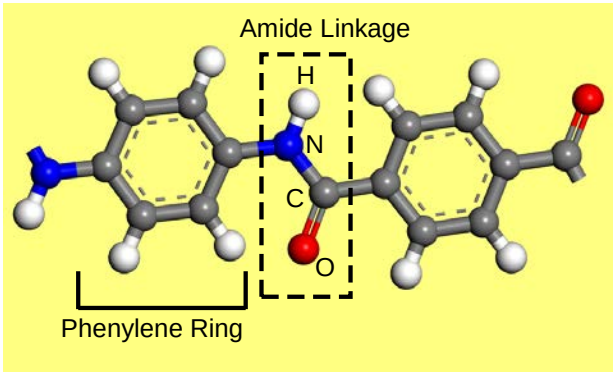

Figure 2. Trans molecular conformations in typical aramid based polymeric material chains/molecules.

Processing induced Defects: As in most engineering materials, properties of PPTA molecules and fibrils (as well as fibers, yarns, etc.) are greatly affected by the presence of various crystallographic and morphological defects. A detailed analysis of the most common PPTA fiber/fibril defects, their character and dimensionality, their cause (i.e. the synthesis and fabrication processes responsible for their formation), ways of reducing their number density and their typical concentrations can be found in [3].

Modeling: Discrete material models and simulations (e.g. molecular statics, MS, and molecular dynamics, MD) are used to infer the constitutive behavior of the reinforcing filaments at the molecular and fibril length scales, and to obtain insight into the effect of various microstructural features (including defects) on this behavior. In general, the formulation of a molecular /fibril level simulation problem requires, at a minimum, specification of the following five items: (a) a molecular level computational model consisting of atoms, ions, moieties and functional groups; (b) a set of force field functions (COMPASS [5], in the present work), which describe various bonding and non-bonding interactions between the constituents of the molecular scale model; (c) types and sequence of the computational method(s) (MS/MD) to be used in the simulation; (d) formulation of the physical problem being investigated/simulated; and (e) specification of the methods and procedures to be used in the post processing data reduction analysis.

To gain insight into the basic microstructure property relations at the molecule and fibril length scales, a relatively large number of molecular level computational models containing various perfect crystal PPTA conformations and different microstructural defects have been used. Figures 3(a)–(d) depict several such computational models. Construction of the defect free PPTA computational material models was carried out under the following conditions: (a) the fibers (not modeled explicitly) are treated as bundles of parallel, fully crystalline fibrils; (b) the crystalline structure of the PPTA fibrils is modeled as a stack of parallel PPTA sheets (formed by hydrogen bonding between nearly parallel PPTA molecular chains, all aligned in the fiber/fibril axis direction); and (c) to account for the fact that the vast majority of the molecules inside PPTA fibrils are fully surrounded by other chains a bulk like environment is created using the concept of the computational cell and the periodic boundary conditions. The computational cells used were all of the rectangular parallelepiped shape, with one of the computational cell edges aligned with the fiber axis. The other two computational cell edges lie in the PPTA sheet and orthogonal to it, respectively.

Virtual Mechanical Tests: MS/MD analyses are used in the present work to simulate different (molecular /fibril scale) mechanical tests, and to determine the associated material properties. The mechanical tests used involve axial tension/compression, transverse compression, transverse shear, axial torsion, etc. Since PPTA fiber diameter is on the order of 10 μm, it is 10^3–10^4 times larger than the lateral edge length of the molecular level computational cells used. Furthermore, fibers are typically composed of several hundreds of axially aligned fibrils. Thus, a PPTA material domain of the size equal to that of the computational cell used has the highest probability of residing within a single PPTA fibril. For this reason, the computational cells used in the simulations of the mechanical tests are assumed to contain perfect or imperfect single crystalline material, and the associated virtual mechanical tests to yield fibril properties.

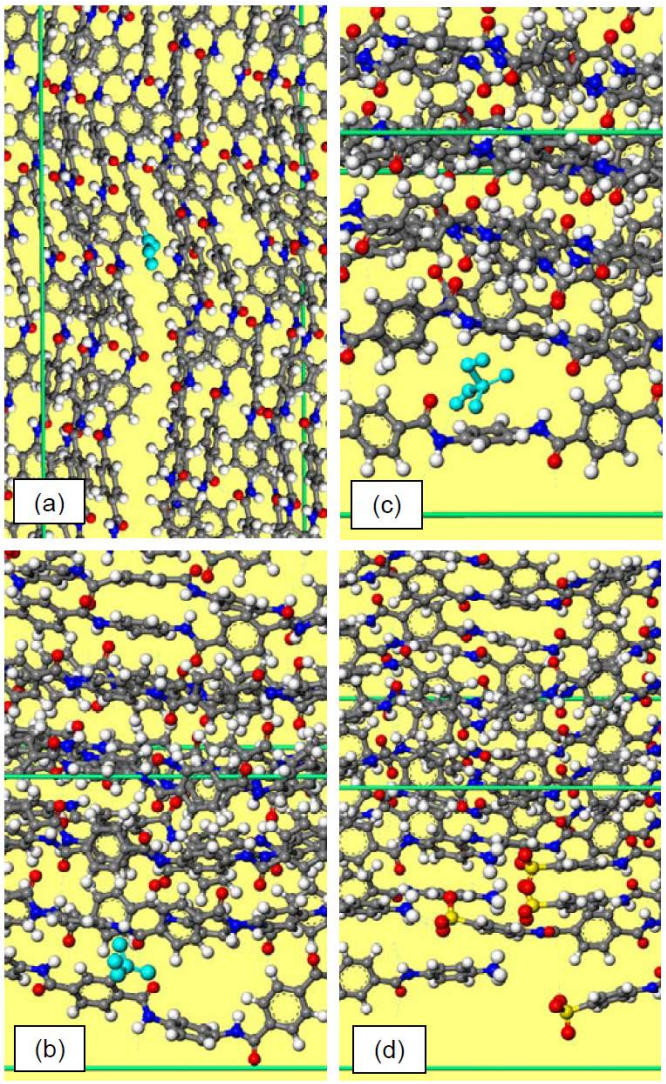

Figure 3. Examples of the computational models containing defective PPTA crystalline structures: (a) isolated –COOH group (a chain end defect); (b) isolated $–SO_3H$ group (a side group defect); (c) isolated mobile H_2SO_4 molecule (an interstitial defect); and (d) a defect band (a planar defect). For clarity, atoms within defects are enlarged and highlighted in cyan in (a)–(c), and enlarged in (d).

In the case of low rate mechanical tests, the following three step procedure was employed: (a) loading was applied in an incremental fashion; (b) each loading step was followed first by a MS potential energy minimization step; and (c) the statically equilibrated material was then dynamically relaxed by subjecting it to a prolonged (ca. 50 ns) equilibrium MD simulation. In the case of high rate mechanical tests, non-equilibrium MD was employed and no potential energy minimization or dynamic relaxation techniques were used.

Data Reduction and Analysis: The results obtained, either under low rate or high rate loading conditions contained the history of the interacting particles' positions, velocities and forces. These results are subsequently processed in order to extract the essential features of the material response when it is subjected to different types of loading at different imposed loading rates. In addition, deformed microstructure is examined in great detail and correlated with the material mechanical properties (primarily stiffness and strength) in order to help establish microstructure

property relations.

To account for non zero temperature and entropic effects, the components of the fourth order elastic stiffness tensor were determined using MD simulation results. Within this procedure, particle trajectory results were first used to determine the ensemble average for the material stress and strain (both treated as second order tensors). Then, using the time based correlation functions between the stress and strain tensors, all the components of the stiffness tensor were determined [3] and, through the use of the Voigt reduced notation, converted into a (6x6) material stiffness matrix. The results obtained revealed nine independent elastic stiffness constants, suggesting the PPTA crystal structure possesses orthotropic symmetry. Using standard mathematical relations, the results were expressed in terms of the three Young's moduli (E_{11}, E_{22}, E_{33}), three shear moduli (G_{12}, G_{13}, G_{23}), and three Poisson's ratios ν_{12} ($=\nu_{21}*E_{11}/E_{22}$), ν_{13} ($=\nu_{31}*E_{11}/E_{33}$) and ν_{23} ($=\nu_{32}*E_{22}/E_{33}$). The three principal (i.e. computational cell edge) directions were respectively aligned with: (a) the fibril/fiber longitudinal direction, x_1; (b) the sheet normal direction, x_2; and (c) the corresponding in sheet orthogonal direction, x_3. As far as the material strength (under different loading modes) is concerned, it was determined by conducting repeated loading and unloading mechanical tests to progressively higher imposed strains and identifying the minimum stress level (for a given type of loading) which produces an irreversible/inelastic strain [5].

Results: Figures 4(a)–(d) show, respectively, the effect of the concentration of a –COOH chain end group, a $-SO_3H$ side group, a mobile H_2SO_4 molecule and a defect band on the relative change in the nine orthotropic elastic moduli with respect to their values in the defect free fibrils (E_{11}=105.3 GPa, E_{22}=2.0 GPa, E_{33}=31.3 GPa, G_{12}=0.9 GPa, G_{13}=5.6 GPa, G_{23}=2.6 GPa, ν_{12}=0.46, ν_{13}=0.147 and ν_{23}=0.15). Examination of Figures 4(a)–(d), reveals that: (a) the orthotropic elastic moduli change monotonically with an increase in the defect concentrations; (b) the longitudinal normal stiffness (E_{11}) and the inter sheet shear stiffness (G_{12}) are most strongly affected/compromised by the presence of the chain end defects, Figure 4(a); (c) in the case of side group defects, Figure 4(b), trans sheet normal stiffness increases either strongly due to establishment of inter sheet hydrogen bonds. Figure 4(b) further reveals that the shear moduli G_{12} and G_{13} are also increased due to the presence of hydrogen bonding; and (d) the presence of interstitial defects has a highly detrimental longitudinal stiffness reducing effect, Figure 4(c). This effect is even more pronounced in the case of defect bands, Figure 4(d). To predict the mean values of the orthotropic elastic constants in fibrils in the commercially produced PPTA fibers, the following deterministic procedure was employed: (a) for each of the microstructural/topological defects analyzed, a mean value of the defect concentration (and its typical range) under prototypical PPTA fiber fabrication conditions is assessed using the available open literature reports; (b) due to the very low values of the defect concentrations, it is assumed that the combined effects of different defects can be obtained using a simple linear superposition procedure; and (c) the effect of individual defects on the fibril orthotropic elastic moduli is assumed to be represented by the results like the ones displayed in Figures 4(a)–(d).

The PPTA fibril longitudinal tensile strength results obtained revealed: (a) a fairly reproducible value of 6.3 GPa in perfect PPTA fibrils; (b) the strength in defective PPTA fibrils is controlled by the size and composition of the largest (i.e. the most potent) defect or defect cluster; and (c) the strength of defective PPTA fibrils is a stochastic quantity, whose probability distribution function is determined using the following procedure: (i) defect distribution within the fibrils is

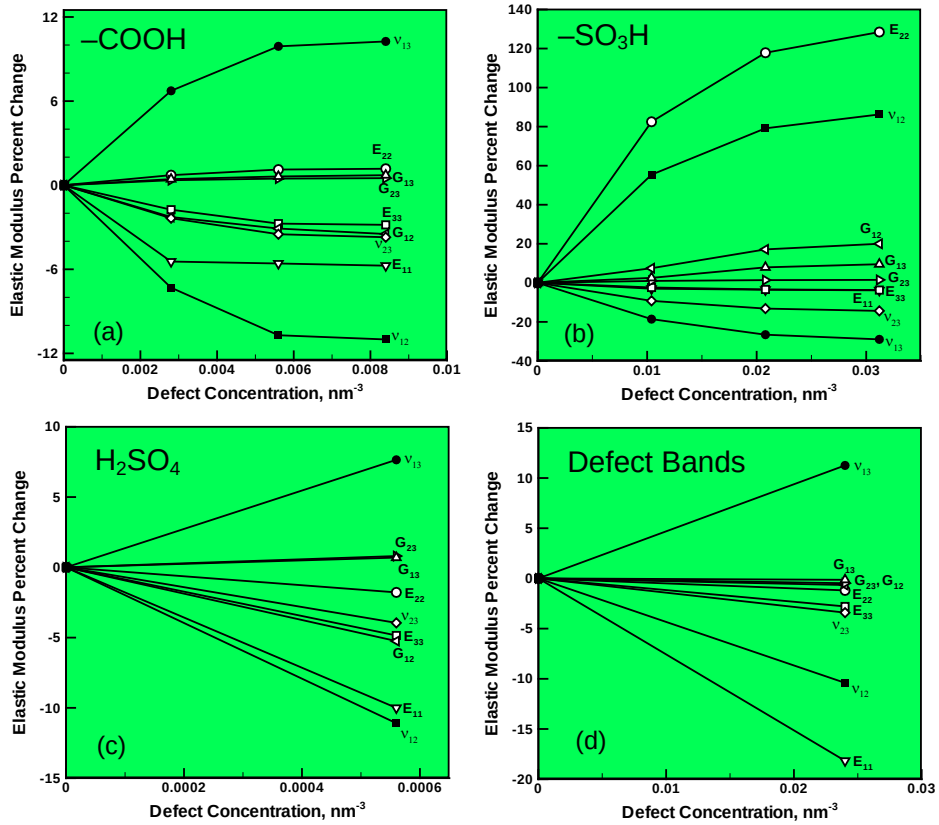

Figure 4. The effect of the concentration of the: (a) –COOH chain end group; (b) $–SO_3H$ side group; (c) mobile H_2SO_4 molecules; and (d) defect bands on the orthotropic elastic moduli of the PPTA fibrils.

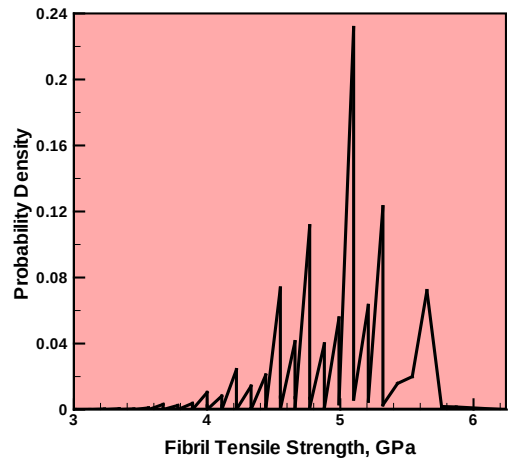

Figure 5. PPTA fibril longitudinal strength probability density function.

assumed to follow the principles of a Poisson point process; (ii) the concept of "*volume of influence*" is next introduced in order to establish a criterion for declaring an ensemble of closely spaced individual defects as a single (high potency) defect cluster; (iii) the defect concentrations associated with the prototypical PPTA fiber fabrication conditions are then assumed; (iv) a large number of (defective PPTA fibril) models are created stochastically and for each case, the corresponding longitudinal strength determined using the procedure described earlier; and (v) the results obtained are finally processed using a statistical probability analysis. This procedure yielded the probability density function displayed in Figure 5. Examination of the results displayed in this figure and the fact that the measured PPTA fibril longitudinal tensile strength is typically found to be in a 3–5 GPa range [e.g. 6], suggests that the computational procedure employed is fairly reliable. Similar findings (not reported for brevity) were obtained for the cases of (buckling controlled) compressive strength as well as for the compressive and shear transverse strengths of the PPTA fibrils.

3. FIBER, YARN AND FABRIC LEVEL MODELING

Fiber level: Since fibers are treated as (continuum) entities consisting of parallel stretched out fibrils, laterally bonded by van der Waals forces, Figure 6(a), the fiber properties are derived by proper statistical averaging of the corresponding fibril properties. Application of such a procedure to the PPTA fiber/fiber stiffness revealed: (a) due to random orientation of fibril sheet normals (within a plane normal to the fiber axis) the PPTA fibers are found to be transversely isotropic (with the fiber axis being the unique material direction); (b) in the axial direction, the fiber normal stiffness, E_{11}, is quite comparable with its fibril counterpart; (c) in the transverse direction, the normal stiffness properties, E_{22}=E_{33}, are found to be close to the more compliant E_{33} Young's modulus of the fibrils; (d) fiber G_{23} shear modulus takes on a value close to its fibril counterpart; and (e) the two remaining fiber shear moduli G_{12} and G_{13} are found to have nearly identical values, the values which are somewhat higher than the fibril G_{12} shear modulus (the modulus which controls the compliant PPTA inter sheet sliding). Application of the aforementioned averaging procedure to the PPTA fiber strength (under different loading conditions) revealed: (a) the longitudinal strength of the fibers and its distribution are quite comparable to their fibril counterparts; (b) the fiber transverse strength is plane isotropic with a mean value slightly higher than the lowest fibril transverse strength; and (c) fiber shear strength is fairly isotropic with an average value comparable to the mean shear strength of the fibril.

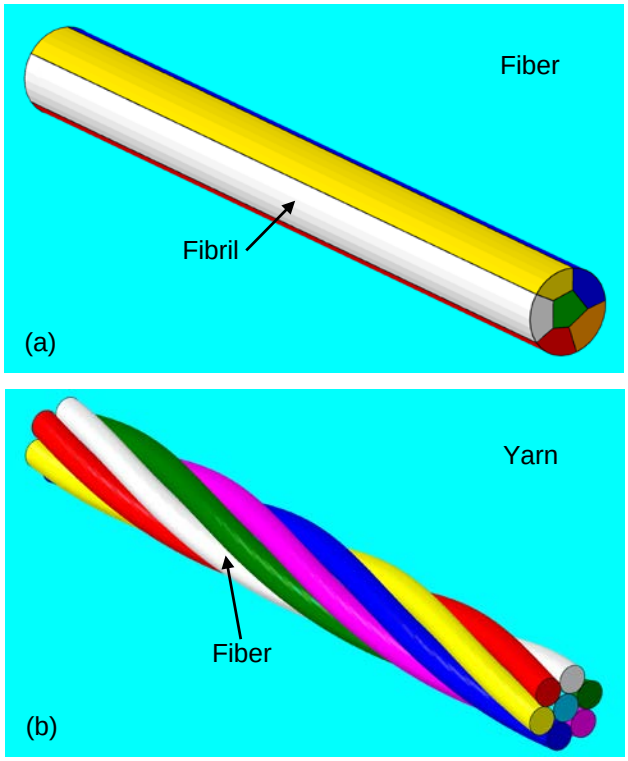

Figure 6. Topological relationships between: (a) PPTA fibrils within a single fiber; and (b) multi fiber lightly twisted yarns.

Yarn level: Yarns represent an assembly of nearly parallel fibers which are mechanically engaged by either light twisting of, or wrapping a fiber around, the fiber assembly, Figure 6(b). Within the present work mechanical properties of the yarns are determined using finite element simulation based virtual mechanical tests in which: (a) yarn internal fiber based architecture is accounted for explicitly; (b) fiber material properties are inherited from the fiber length scale analysis (described above); and (c) the phenomena such as fiber/fiber friction and fiber juxtaposition are accounted for explicitly. Examination of the results yielded by such finite element analysis revealed that PPTA yarns: (a) behave as transversely isotropic structures/materials; (b) the material behavior is nearly linear elastic up to the point of fracture; and (c) the five transversely isotropic elastic moduli for the PPTA yarns are characterized by: (i) the axial elastic modulus, E_{11}, is increased relative to its fiber counterpart by an amount

proportional to the extent of yarn twisting. This increase reflects the contribution associated with inter fiber friction arising from the twist applied to the yarn in order to engage the fibers, and reveals the fact that the yarn level material properties are dependent on the fibril/fiber (crystallographic/morphological defects controlled) properties as well as on the details of yarn architecture (e.g. the extent of fiber twist); (ii) the transverse elastic moduli, $E_{22}=E_{33}$, generally acquire values which are only a small fraction of the axial Young's modulus, which can be linked to the relatively weak transverse inter fiber bonding; (iii) all shear moduli acquire quite small values, as a result of the interplay of fiber juxtaposition; and (iv) all Poisson's ratios acquire values near 0.0, due to the fact that the yarn is an assembly of discrete fibers. Consequently, fibers can experience Poisson's effects without the yarn experiencing these effects. Further examination of the finite element results revealed that: (a) the mean longitudinal tensile and compressive yarn strengths are slightly (by ca. 0.2/0.3 GPa) increased relative to their fiber counterparts, while the associated standard deviations are smaller; (b) the transverse (compressive) strength of the yarn is quite comparable to its fiber counterpart; and (c) yarn transverse shear strength is somewhat higher than its fiber counterpart.

Fabric level: At this level, the contributions of the yarn material properties and the fabric architecture (e.g. plain weaving, etc.) are combined. This is accomplished by constructing, parameterizing and virtual testing of a "meso scale" planar shell based fabric unit cell [7, 8]. It should be noted that in order to include the effect of the fabric manufacturing process on the yarn material properties, a distinction is made between the weft and the warp yarns since these two families of yarns experience property degradation (by different amounts) relative to the property levels identified in the yarn level analysis.

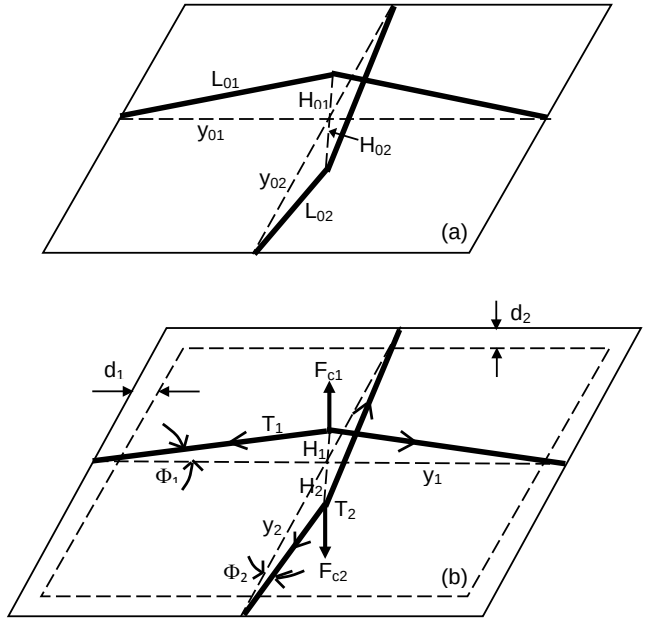

Figure 7. Geometrical representation of a single unit cell for a plain woven single ply fabric: (a) before and (b) after application of a normal biaxial in plane deformation.

A simple schematic of the unit cell which is used to represent the plain woven single ply fabric structure/architecture allotted to a single yarn crossover in its initial (un deformed) configuration is depicted in Figure 7(a). In this figure, the two crossing yarns are simplified as two two-member truss elements each with a cross section that is initially uniform and elliptical. A deformed configuration of the simplified unit cell model is depicted in Figure 7(b).

Examination of this unit cell reveals that: (a) due to the truss character of the yarn elements, the contact between the yarns at the crossover is reduced to a point; (b) when determining the potential contact between the crossing yarns, their instantaneous half thicknesses are taken into account; (c) when the unit cell is stretched in a particular in plane direction, the corresponding yarn is either de-crimped/straightened or stretched. In the former case, no

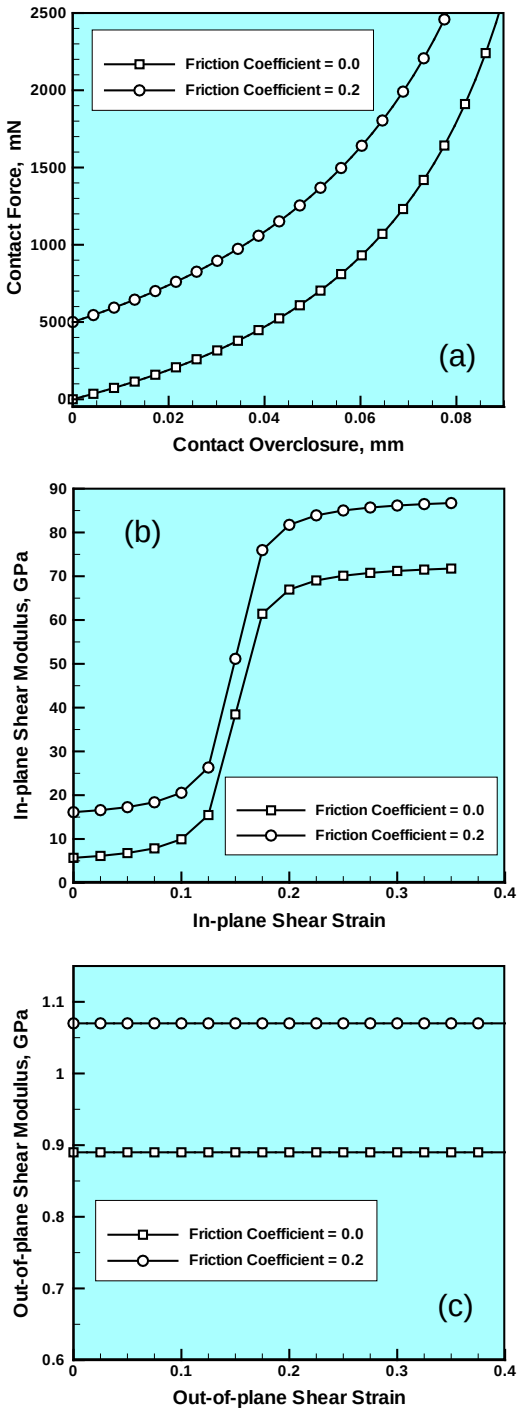

Figure 8. Typical results obtained in three dimensional FEM analyses of the deformation of the single ply fabric unit cell under: (a) in plane biaxial tension; (b) in plane shear; and (c) out of plane/transverse shear.

tension is built within the yarn, while in the latter case tension is created within the yarn and, if sufficiently high, can cause yarn failure; (d) furthermore, the extent of tension in a given yarn is affected by the failure status of the other crossing yarn. For example, if the crossing yarn is unbroken and in contact with the stretched yarn, tension will develop in the two yarns, the extent of which depends on the degree of contact over closure (i.e. the reduction in distance of the two summit points relative to the initial distance) and the functional relationship between the contact over closure and the magnitude of the contact force; (e) due to a lack of yarn/yarn engagement during in plane normal compression fabric in plane compressive strength is governed by the yarn longitudinal compressive strength; and (f) many other phenomena/scenarios are encountered in the fabric unit cell when the cell is subjected to different types of in plane and out of plane loading, the loading which can cause breakage of one of the yarns, yarn crimping, yarn/yarn sliding, etc.

To derive the meso scale fabric type material model for shell elements, the unit cell is subjected to three types of loading: (a) in plane biaxial tension/compression; (b) inplane shear; and (c) out of plane (transverse) shear. For each of these loading conditions, the kinematic response of the unit cell is analyzed and the accompanying phenomena and processes, e.g. yarn tension/crimping, yarn/yarn contact, yarn/yarn sliding are identified. To infer the basic constitutive relations governing these phenomena/processes and to parameterize these relations, a three dimensional solid FEM model of a single unit cell is constructed and subjected to the same type of loading. For example, balanced biaxial in plane tension is used to monitor the evolution of the yarn/yarn contact force as a function of the contact over closure, in order to infer the basic functional form and to parameterize the truss/truss contact force vs. summit point distance constitutive relationship. An example of such a functional relationship is depicted in Figure 8(a). Examples of additional

functional relationships obtained through the application of the in plane shear and out of plane/transverse shear are shown in Figures 8(b)–(c), respectively.

The final outcome of the procedure described in this section is a complete material constitutive model for a single ply of the reinforcing fabric. A constitutive model typically includes a generalized Hooke's law (which governs the stress evolution), an inelastic deformation law (which governs the strain evolution), and a set of material state evolution equations (equations which describe permanent changes in the state of the material during loading).

4. SINGLE & STACKED LAMINA LEVEL MODELING

Single lamina Level: Within this length scale, the single ply fabric material model is combined with the polymeric matrix material model, within a homogenization procedure, to arrive at the effective material model for a single composite material lamina. At this point, the effect of "resin starving" is taken into account. In the present work, a homogenization procedure such as the Voronoi cell based homogenization procedure [9] is employed. The resulting single lamina material model is effectively a polymeric matrix modulated single ply fabric material model described in the previous section.

Stacked lamina Level: Within this type of material model, separate constitutive relations are defined for the single ply laminae (accounts for the response of the material within individual laminae) and for the lamina/lamina interfaces (used to account for potential matrix delamination caused by through the thickness tensile loads and in plane shear), as well as an algorithm for their integration into a laminate level material constitutive response. The single lamina material constitutive model used here is an adaptation, simplification and refinement of the corresponding material model described earlier in this section. Specifically, the single lamina material model used here is assumed (for the sake of computational efficiency) to be of a linear elastic character with degradable elastic moduli. The number of the damage variables used, their evolution equations and the effect of these variables on different elastic moduli are chosen in such a way that the resulting single lamina material model yields the results which are consistent with the ones yielded by the single lamina material model, described earlier in this section. The present single lamina material constitutive model is enriched and further refined under the following basic assumptions and conditions: (a) due to a relatively small lamina thickness, variations of the stress, strain and damage fields through the lamina thickness is ignored; (b) material failure is controlled by progressive damage (resulting from high local in plane tensile and shear stresses) and by quasi brittle fracture (controlled by high local compressive and through the thickness shear stresses); (c) since damage nucleation and evolution are controlled by the growth of the associated material flaws/defects (the velocity of which is limited by a relativistic effect based terminal velocity), the rate of damage evolution is also limited; and (d) the extent of material damage is represented by three scalar internal damage variables: (i) one that affects materials mechanical response in the fiber direction; (ii) one that affects material response in the transverse and in the through the thickness directions; and (iii) one that affects shear response of the laminae. While the first damage variable is directly linked to fiber failure within the yarns, the other two damage variables are assumed to result from all the remaining intra lamina damage processes. The main components of the present single lamina material model are [10]: (a) a set of evolution equations, one for each damage variable; (b) the effect of all three damage variables on each of the single lamina material elastic modulus; (c) contribution of the material damage to,

and its interaction with, inelastic deformation processes; and (d) integration of the material and stress/strain states over an arbitrary loading path/trajectory.

Lamina/lamina interfaces are modeled as three dimensional surface entities. Consequently, the mechanical state of the interface is represented by one normal and two shear stresses (or more precisely, the traction forces). These stresses are taken to depend, in a non linear fashion, on the corresponding interfacial displacement discontinuities (i.e. displacement differences between the two sides of the interface). The associated stress vs. displacement discontinuity functional relations are obtained by differentiating the corresponding interfacial potential function [10]. Under quasi static loading conditions, within the stacked lamina scale material model, evolution of the (mode I, II and III) interfacial damage is assumed to be controlled by the corresponding thermodynamic forces (i.e. energy release rate like quantities). Furthermore, following the standard practice, it is assumed that the three basic modes of interfacial damage are mutually related/coupled. This is accomplished within the model by assuming that the extents of all three basic damage modes depend on a single generalized energy release rate like quantity. Furthermore, through proper selection of the damage extent vs. release rate functional relations, the interfacial response within the model is allowed to become either brittle (instantaneous failure) or ductile (progressive damage and gradual failure). Under dynamic/impact loading conditions, the rate of interfacial damage accumulation is assumed to be limited by the terminal velocity for damage advancement along the interface. It should be noted that, as in the case of the individual laminae, lamina/lamina interfaces are assumed to remain linear elastic during loading, but the associated elastic constants experience continuous degradation as a result of the accompanying damage.

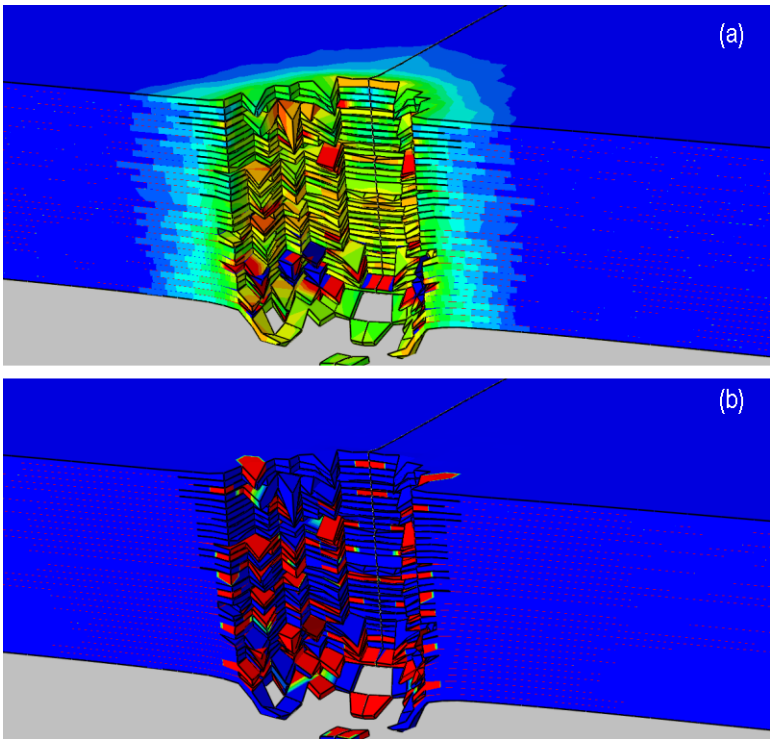

Figure 9. The spatial distribution of damage variables at 30 μm FSP post impact time within the laminate as predicted by the meso scale material model: (a) d_f – Red ≥ 0.05; Blue ≤ 0.005, and (b) d – Red ≥ 0.25; Blue ≤ 0.025.

Results: Examples of the finite element results obtained using the stacked lamina material model for PPTA fabric reinforced polymer matrix composite laminate consisting of 32 laminae and impacted (at a 0° obliquity angle and an incident velocity of 500 m/s) by a 0.30 caliber steel fragment simulating projectile (FSP) are shown in Figures 9(a)–(b). Figures 9(a)–(b) show, respectively, post mortem spatial distribution of two damage variables, d_f, (quantifies the extent of fiber breakage within the yarns) and d' (quantifies the extent of fiber/matrix de-bonding and

diffuse matrix damage). Examination of the results displayed in these figures suggests that fiber breakage, as expected, is the dominant mode of damage in the region around the penetration hole, while fiber matrix (as well as matrix/matrix) delamination is more pronounced in the region near the laminate back face.

5. LAMINATE LEVEL MODELING

In this case, the material is completely homogenized, i.e. the behavior of each material point is assumed to be governed by the same degradable (linear elastic) material constitutive model. It should be noted that despite the fact that the composite material is homogenized, during the derivation of the laminate/continuum scale material models, full recognition is given to the underlying material microstructure as well as to the associated deformation, damage and failure processes. Consequently, formulation and parameterization of this material constitutive model is conducted in close association with the previously reviewed finer scale material models.

Model Foundation: The defining features of the present laminate scale material model are as follows: (a) high strain rate, large strain and high pressure effects are accounted for; (b) the model is strain based and utilizes the concept of a lamina averaged local strain; (c) the model utilizes Mohr-Coulomb [11] shear strength effects, to account for the fact that the (matrix) in plane shear strength is a function of the (tensile/compressive) character and magnitude of the through the thickness lamina strain; (d) the following three fiber and two matrix failure modes are considered: (i) fiber/yarn failure due to a combination of axial tensile and transverse shear strains; (ii) fiber buckling failure due to axial compressive strains; (iii) fiber crushing failure due to lamina through the thickness compressive strains; (iv) matrix in plane shear failure; and (v) matrix delamination failure due to combined effects of the through the thickness tensile strains and transverse shear strains; and (e) the model is essentially of a linear elastic orthotropic type with progressively degradable elastic stiffness constants and, consequently, it requires the definition of the damage initiation criteria and the corresponding damage evolution laws. Damage initiation is defined by a set of seven equations (five damage modes plus for two of these modes, fiber damage under combined axial tension and transverse shear and fiber damage under axial compression, distinction is made between the warp and weft yarns). Each of these equations is in the form: a strain based loading function has to be greater than or equal to the particular damage type material resistance for the damage mode in question to initiate or continue to evolve. Within the strain space, each of these equations defines a damage initiation hyper surface. Since the size of these hyper surfaces scales inversely with the associate material elastic moduli, as damage progresses during loading, these hyper surfaces expand. This expansion is governed by the damage evolution equations while the associated degradation in the elastic moduli is quantified by the appropriate damage variables (where one or more damage modes can contribute to the evolution of a given damage variable). During identification and quantification of different damage/failure modes to each elastic modulus, the following approach is taken: (a) failure of the weft and warp fibers both in tension and transverse shear and in compression degrades the associated Young's modulus and shear moduli; (b) fiber crushing mode degrades all elastic moduli; (c) in the case of the in plane shear failure, only the associated shear modulus is affected; and (d) delamination degrades the through the thickness Young's modulus as well as the two transverse shear moduli.

For the laminate scale material models to be applicable in the ballistic/blast computational

analyses, they must include the effects of loading rate on the material stiffness and strength. These rate sensitivity effects are included through the use of appropriate thermal activation based laws [11]. The accompanying thermal effects are accounted for through the use of temperature dependent material parameters and by assuming adiabatic conditions. That is, due to the short duration of the blast/ballistic impact events, the effects of heat conduction (and other heat transfer modes) is neglected.

Results: In Figures 10(a)-(d), a set of finite element results is presented pertaining to the spatial distribution of the composite material (modeled using the laminate scale material model) being impacted transversely by a right circular cylindrical rigid projectile at a 0° obliquity angle. It should be noted that in order to enable monitoring of the penetration process, the target plate is made transparent. The results displayed in Figures 10(a)-(d) clearly reveal the development of the back face bulge (the magnitude of which is consistent with its experimental counterpart reported in [11]).

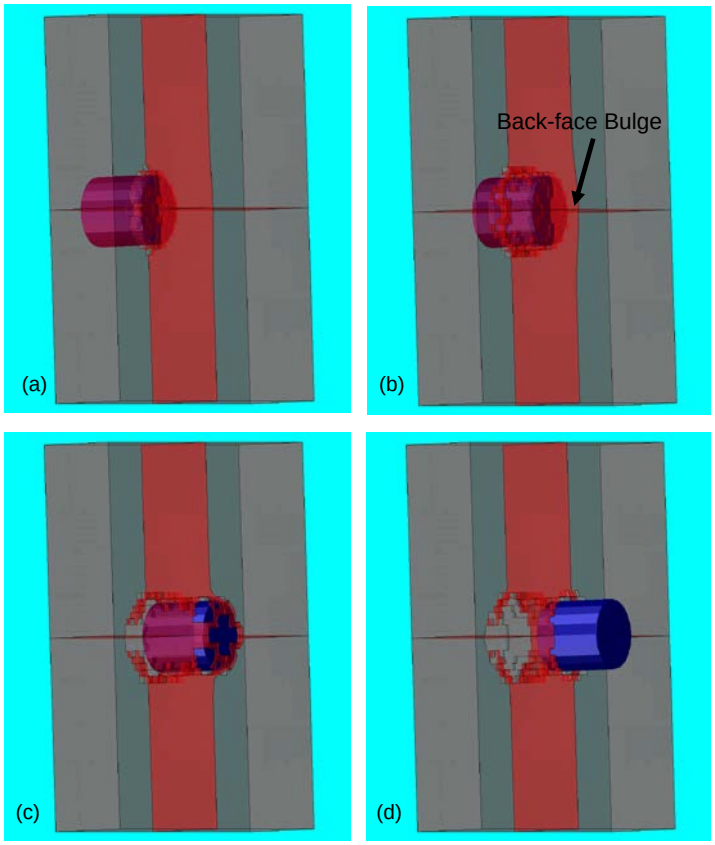

Figure 10. Typical results pertaining to the temporal evolution of the spatial distribution of the composite laminate material during impact by a right circular cylindrical rigid projectile.

By carrying out a simple sensitivity analysis, it was demonstrated in the present work that details regarding the spatial distribution of the material during impact as well as the overall penetration resistance of the composite laminate can be greatly affected by the choice of the functional forms and the parameterization of the constitutive relations governing the kinematic and mechanical response of the composite laminate material. This finding justifies the use of a comprehensive multi length scale computational approach, like the one developed in the present work, for inferring and calibrating such relationships.

6. CONCLUDING REMARKS

While the present work was focused on PPTA based filaments and the associated AGCs, the approach and methodology could be readily extended to other classes of polymer matrix composites. The PPTA based system was selected for two main reasons: (a) to display the full richness of the hierarchical nature of the material microstructure and properties; and (b) to be able, within the limited space available, to highlight some specific aspects of the material

microstructure and behavior at different length scales.

7. REFERENCES

1. Grujicic, M., Glomski, P. S., He, T., Arakere, G., Bell, W. C. & Cheeseman, B. A. "Material Modeling and Ballistic-resistance Analysis of Armor-Grade Composites Reinforced with High-Performance Fibers." *Journal of Materials Engineering and Performance* 18 (2009): 1169–1182.
2. Grujicic, M., Bell, W. C., Glomski, P. S., Pandurangan, B., Yen, C.-F. & Cheeseman, B. A. "Filament-level Modeling of Aramid-based High-Performance Structural Materials." *Journal of Materials Engineering and Performance* 20 (2011): 1401–1413.
3. Grujicic, M., Bell, W. C., Glomski, P. S., Pandurangan, B., Yen, C.-F. & Cheeseman, B. A. "Multi-length Scale Computational Derivation of Kevlar® Yarn-level Material Model." *Journal of Materials Science* 46 (2011): 4787–4802.
4. Grujicic, M., Ramaswami, S., Snipes, J. S., Yavari, R., Lickfield, G. C., Yen C.-F. & Cheeseman, B. A. "Molecular-Level Computational Investigation of Mechanical Transverse Behavior of p-phenylene terephthalamide (PPTA) Fibers." *Multidiscipline Modeling in Materials and Structures* 9 (2013): 462–498.
5. Grujicic, M., Yavari, R., Snipes, J. S., Ramaswami, S., Yen, C.-F. & Cheeseman, B. A. "Molecular-Level Study of the Effect of Prior Axial Compression/Torsion on the Axial-Tensile Strength of PPTA Fibers." *Journal of Materials Engineering and Performance* 22 (2013): 3269–3287.
6. Grujicic, M., Ramaswami, S., Snipes, J. S., Yavari, R., Yen, C.-F. & Cheeseman, B. A. "Axial-Compressive Behavior, Including Kink-Band Formation and Propagation, of Single p-Phenylene Terephthalamide (PPTA) Fibers." *Advances in Materials Science and Engineering*, Volume 2013, Article ID 329549, 2013.
7. Grujicic, M., Bell, W. C., Arakere, G., He, T., Xie, X. & Cheeseman, B. A. "Development of a Meso-scale Material Model for Ballistic Fabric and its Use in Flexible-armor Protection Systems." *Journal of Materials Engineering and Performance* 19 (2010): 22–39.
8. Grujicic, M., Bell, W. C., He, T. & Cheeseman, B. A. "Development and Verification of a Meso-scale based Dynamic Material Model for Plain-woven Single-ply Ballistic Fabric." *Journal of Material Science* 43 (2008): 6301–6323.
9. Grujicic, M., Hariharan, A., Pandurangan, B., Yen, C-.F., Cheeseman, B. A., Wang, Y., Miao, Y. & Zheng, J. Q. "Fiber-level Modeling of Dynamic Strength of Kevlar® KM2 Ballistic Fabric." *Journal of Materials Engineering and Performance* 21 (2012): 1107–1119.
10. Grujicic, M., He, T., Marvi, H., Cheeseman, B. A. & Yen, C.-F. "A Comparative Investigation of the Use of Laminate-level Meso-scale and Fracture-mechanics Enriched Meso-scale Composite-material Models in Ballistic-resistance Analyses." *Journal of Materials Science* 45 (2010): 3136–3150.
11. Grujicic, M., Pandurangan, B., Snipes, J. S., Yen, C-F. & Cheeseman, B. A. "Multi-Length Scale Enriched Continuum-Level Material Model for Kevlar®-Fiber Reinforced Polymer-Matrix Composites" *Journal of Materials Engineering and Performance* 22 (2013): 681-695.